Experiments in Fluids (2006) 40: 70–79
DOI 10.1007/s00348-005-0047-z

RESEARCH ARTICLE

A. Susset · J. M. Most · D. Honoré

A novel architecture for a super-resolution PIV algorithm developed for the improvement of the resolution of large velocity gradient measurements

Received: 9 November 2004 / Revised: 8 August 2005 / Accepted: 17 August 2005 / Published online: 5 October 2005

Abstract Three different particle image processing algorithms have been developed for the improvement of PIV velocity measurements characterized by large velocity gradients. The objectives of this study are to point out the limitations of the standard processing methods and to propose a complete algorithm to enhance the measurement accuracy. The heart of the PIV image processing is a direct cross-correlation calculation in order to obtain complete flexibility in the choice of the size and the shape of the interrogation window (IW). An iterative procedure is then applied for the reduction of the size of IW at each measurement location. This procedure allows taking into account the local particle concentration in the image. The results of this first iterative processing, applied to synthetic images, show both a significant improvement of measurement accuracy and an increase of the spatial resolution. Finally, a super-resolution algorithm is developed to further increase the spatial resolution of the measurement by determining the displacement of each particle. The computer time for a complete image processing is optimized by the introduction of original data storage in Binary Space Partitions trees. It is shown that measurement errors for large velocity gradient flows are similar to those obtained in simpler cases with uniform translation displacements. This last result validates the ability of the developed super-resolution algorithm for the aerodynamic characterization of large velocity gradient flows.

A. Susset · J. M. Most
LCD – UPR, 9028 CNRS ENSMA,
86960 Futuroscope, France

Present address: A. Susset
R&D Vision, 14 rue Soleillet, 75020 Paris, France

D. Honoré (✉)
CORIA–UMR 6614 CNRS,
Université et INSA de Rouen, Technopôle du Madrillet,
76801 Saint Etienne du Rouvray, France
E-mail: david.honore@coria.fr
Tel.: +33-2-32959852
Fax: +33-2-32959780

Keywords Laser diagnostic · Velocity · PIV · Super-resolution · Synthetic image · Binary space partition

1 Introduction

Nowadays, Particle Image Velocimetry is a very useful tool for the determination of the aerodynamic field of complex flows. However, it still suffers from a lack of accuracy in cases of flows characterized by large velocity gradients. The first goal of this work was to develop a new PIV algorithm particularly well adapted for the study of turbulent flames generated by bluff-body or swirl burners characterized by internal recirculation zones and where counter-flows and vortices can co-exist with large velocity gradients (Honoré et al. 2000). Then, in order to improve the velocity measurement accuracy, an original PIV algorithm has been developed on the base of a direct calculation of the cross-correlation (CC) function in order to allow a large flexibility in the choice of the size and shape of the interrogation windows (IW) without systematically using FFT based algorithms. To validate this procedure, a parametric study was performed on synthetic images with constant particle displacements and a comparison with classical FFT algorithms was done (Susset et al. 2000). Even if the results are enhanced, the computational time for a direct cross-correlation calculation still remains long. Some authors have tried to increase the processing speed by compressing the images (Hart 1998) or by performing only a part of the calculation (Roth and Katz 2001). An other approach is proposed in the present work leading to a CC computational time comparable to a FFT one as well as the improvement of the spatial resolution of the measurement. An iterative scheme for the direct CC algorithm is developed with a reduction of the interrogation window size, followed by an ultimate super spatial resolution algorithm to generate one displacement measurement for each particle in the image.

2 Speeding-up method for direct CC calculations

The PIV method assumes that the particle displacement in each interrogation window (IW) is deduced from the position of the CC function peak. In order to decrease the CC computational time, the processing must minimize the number of multiplication operations, which are longer than the addition ones. For this purpose, original data storage has been searched. Usually, an IW is described as a M x N pixel^2 matrix where each couple (i; j)—ranging respectively between [0; M-1] and [0; N-1]—has a value associated to its grey level k ranges from 0 to (2^p-1), where p is the image dynamics. A basic calculation of the direct CC between two $M \times N$ pixel^2 IW induces $(M \times N)^2$ multiplications and $(M \times N)^2$ additions. In the proposed procedure, the number of multiplications is decreased thanks to a new data structure for each IW. As shown in Fig. 1, it consists of defining a NVG(k) vector including the k grey levels from k_{min} to k_{max} associated to the three data fields. The first one contains an integer NB_k representing the number of pixels in the IW where the grey level is k, whereas the second and third data contain the corresponding (i; j) pixel positions.

Such a structure is created for each of the two IW of the direct CC calculation. As a first advantage, the number of multiplications decreases drastically. For example, if we consider two 32×32 pixel^2 IW with grey levels in the range [0; 255] (i.e. 8 bit images), the total number of multiplications will be (256×256) = 65,536 instead of $(32 \times 32)^2$ = 1,048,576 with a classic approach. The operations required for a complete CC calculation are only additions and indice shifts that saves 20% of the average computer time. However, the computational time remains still prohibitive for large amount of data. For example, only 12 vectors/s are determined for 32×32 pixel^2 IW using a 750-MHz processor, compared to more than 500 vectors/s for FFT algorithms.

The main advantage of this new data storage structure is that it classifies information from the lowest k_{min} to the highest grey level k_{max}. Generally, the scattering signal of particles is assumed to high grey levels whereas background and noise to the lowest ones. Therefore, a sweeping of the structure from k_{max} to k_{min} enhances the signal processing (CC function peak) instead of the noise. This procedure is kept dynamically during the scanning. Figure 2 compares the two methods of construction of the CC peak as a function of the percentage of pixels processed in a 32×32 pixel^2 IW. The left graphs correspond to the conventional processing scheme where CC calculations are performed pixel by pixel in 4 interleaved loops whereas the right graphs use the new data structure from k_{max} to k_{min}. It can be observed that at half of complete computational time, the height of the CC peak reached 50% of the final one with the usual processing and 94% with this new data structure. The calculation is stopped as soon as the peak position remains fixed during several iterations on successive grey levels. For example, on Fig. 2, the final position of the CC peak is reached after 10% of the processed pixels and the calculation is then stopped. This procedure drastically decreases the computational time without any loss of CC quality. In these conditions, the processing speed is not prohibitive: the complete direct CC calculation time becomes similar or sometimes even smaller than those from FFT based algorithms.

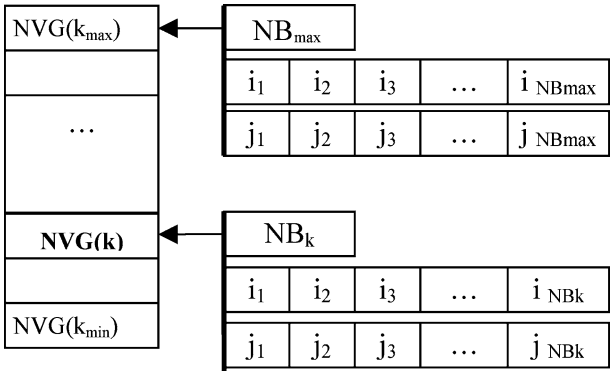

Fig. 1 Diagram of data structure adopted for each IW

When the particle displacement is much larger than the IW size, the CC function peak cannot be detected as its amplitude decreases with the number of products contributing to its building. This effect can be limited by implementing a corrective calculation step: the IW of the second image is shifted by an integer value corresponding to the displacement determined at the first iteration, the CC function peak is then centred in the correlation space. A residual displacement, determined by a sub-pixel Gaussian interpolation, is added to the IW shift. Such an operation, permitting a catching up with the particles, is common in PIV algorithms. This processing is designated as the standard processing.

3 Resolution of velocity gradients by standard processing

The accuracy of the direct CC processing is evaluated on synthetic particle images. For this purpose, a synthetic image builder has been developed to generate particle image batches corresponding to different motion configurations. Translation, rotation or other displacements can be selected to evaluate the accuracy and the limitations of the proposed PIV algorithm. A normal distribution is chosen for grey level repartition of particle scattering intensity, the dynamic of synthetic images is fixed at 8 bits and other advanced functionalities allow the generation of realistic synthetic images, for example the loading of a displacement field and / or a user defined particle distribution (Susset 2002).

The standard processing has first been evaluated on these synthetic images with a uniform translation of the particle displacements: the global measurement errors are less than 0.1 pixel (Susset et al. 2000). In order to apply this approach to complex flows such as turbulent

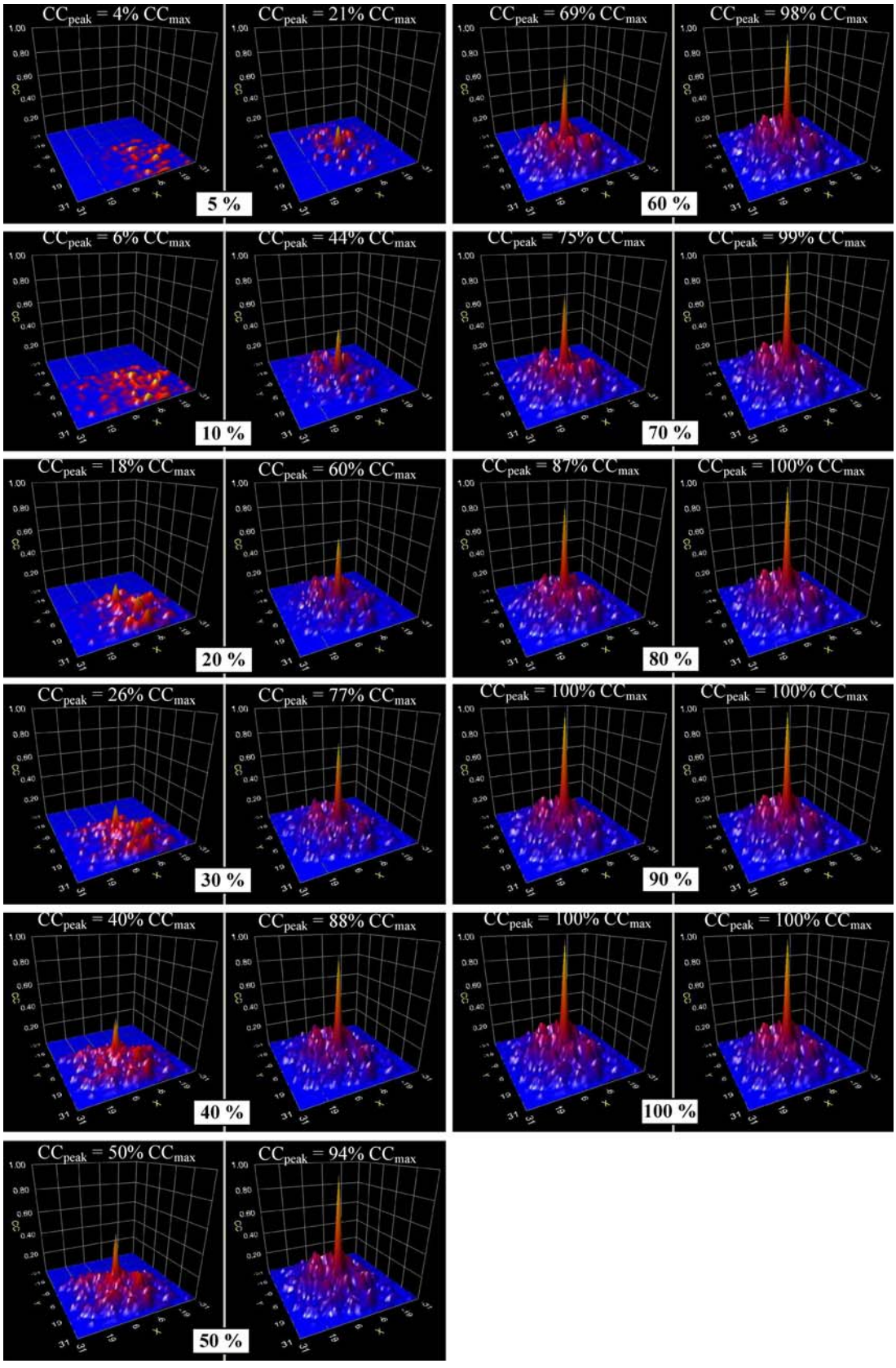

Fig. 2 Dynamic construction of the CC peak as function of the percentage of pixels processed in the IW, calculated with the ''pixel by pixel'' conventional processing (*left*), and with the new data storage structure processing (*right*)

flames (Susset et al. 1998, Honoré et al. 2000), the processing accuracy has been evaluated on large velocity gradient flows. Such a configuration is modelled with synthetic images with a linear displacement gradient along the horizontal axis and zero along the vertical one. Any particle displacement is imposed on the horizontal axis and the particle distribution is randomly determined. No out-of-plane motion of particles is considered in the present synthetic images in order to isolate the effect of local velocity gradient on the PIV measurement. The value of the imposed gradient, S_{imp}, is defined as the ratio of the maximum velocity difference on the image width and varies from 0.05 to 0.5 in the present case. For each value of S_{imp}, 7,000 independent measurements are performed to ensure the convergence of the statistical study. Figure 3a represents an example of a synthetic image and the corresponding displacement field for $S_{imp} = 0.2$, i.e. a vertical displacement difference of 14 pixel over the 70 pixel width of the image. The associated mean displacement profile, averaged over the height of this image, is shown on Fig. 3b.

The size of the interrogation windows is 20×60 pixel^2 including an average of 30 particles with a mean size of 4 pixels. The measured displacement gradients S_{mes} are obtained from a linear regression of the average displacement of the horizontal profiles. Figure 4 represents this evolution as function of the imposed displacement gradient S_{imp}. A linear regression is applied to the set of S_{mes} points in Fig. 4, the resulting slope—equal to 0.9515—shows an underestimation of the standard processing in the studied range. Figure 5 shows the increase of the RMS value of S_{mes} as function of the imposed displacement gradient S_{imp}: the maximum value for the highest tested gradient (2.5 pixel for $S_{imp} = 0.5$) is 25 times greater than that in the case of translation displacements (Susset et al. 2000). This reveals that standard processing induces errors, which are too large for application on flows with large velocity gradients.

4 The iterative processing

4.1 Principle of the IW resizing in the iterative method

Different methods have been suggested by several authors for the improvement of PIV measurements in large velocity gradient flows. They can be grouped into three categories: i] methods using morphology of the CC function (Roth and Katz 2001), ii] methods based on image shape adaptation (Huang et al. 1993, Tokumaru and Dimotakis 1995; Quénot et al. 1998; Ishikawa et al. 2000) and iii] methods using an iterative IW sizing (Lecordier 1997; Scarano and Riethmuller 1999). In the present study, an IW re-sizing method has been adopted, allowing enhancement of the spatial resolution on top of the improvement of the measurement accuracy. The choice of a direct CC calculation is particularly adapted to IW re-sizing because it does not place any restriction on the IW shape unlike with standard FFT-based algorithms. This approach is implemented in an iterative procedure by a predictor / corrector scheme (Fig. 6).

Three successive processing methods can be isolated in the global iterative scheme. The initialization consists of the determination of the displacement field on a coarse grid by a standard processing with large IW, four times larger than the expected maximum displacement. The displacement field is determined in the second step on a finer grid—supposed to be the final grid—after displacement validation and spurious vector interpolation. As the standard processing, this predictor stage is followed first by an integer shifting of the second image of the same IW and then by a sub-pixel Gaussian interpolation. The results are validated by global and local filterings with spurious vector interpolation.

Always in the iterative procedure, the IW size is decreased by a dichotomic area reduction dependent of the validation result. The surface of the IW of a validated displacement is multiplied by 0.50 (i.e. half area),

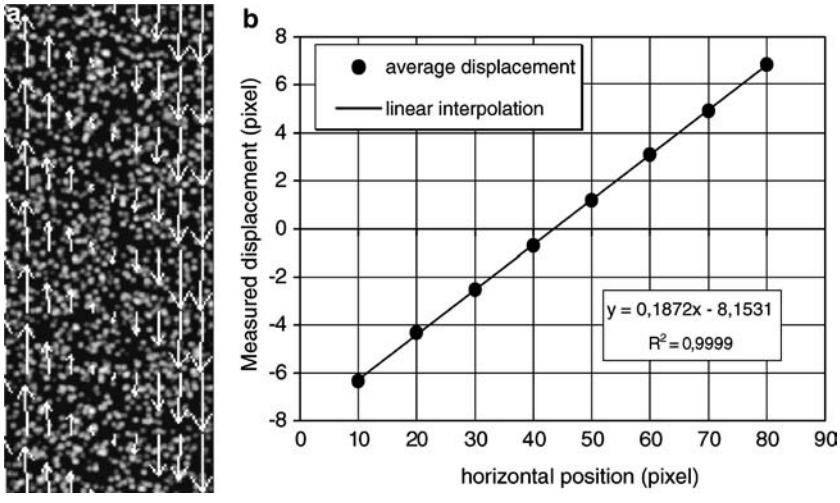

Fig. 3 Example of processing of a pair of synthetic images for Simp = 0.2 **a** synthetic image and corresponding displacement field, **b** average displacement profile

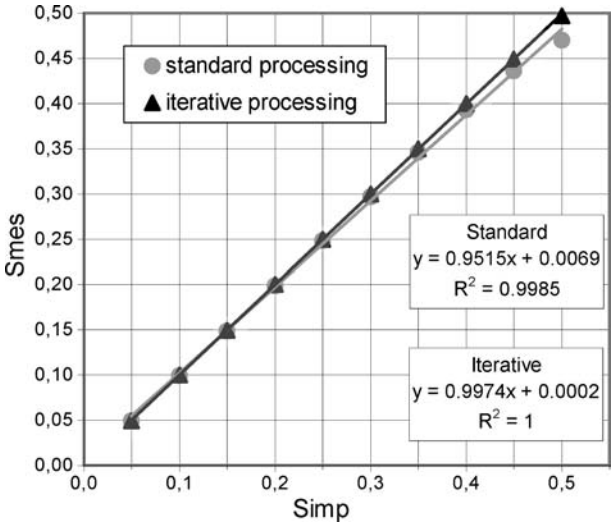

Fig. 4 Measured displacement gradient versus imposed displacement gradient

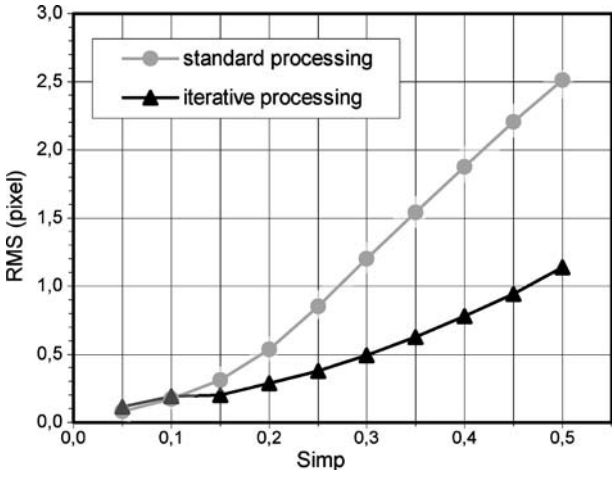

Fig. 5 RMS of measured displacement versus imposed displacement gradient

whereas the surface of the IW with spurious vector is multiplied by 0.75. Keeping the same measurement location grid, the calculations of the predictor/corrector are then performed for each IW with these new dimensions. The criteria to stop the iterative reduction is defined as either the IW reaches a minimum size of 8×8 pixel^2, or the IW area reduction is less than 10% between two successive iterations. The main specificity of this iterative procedure is that the dichotomic size reduction is performed independently for each IW. This

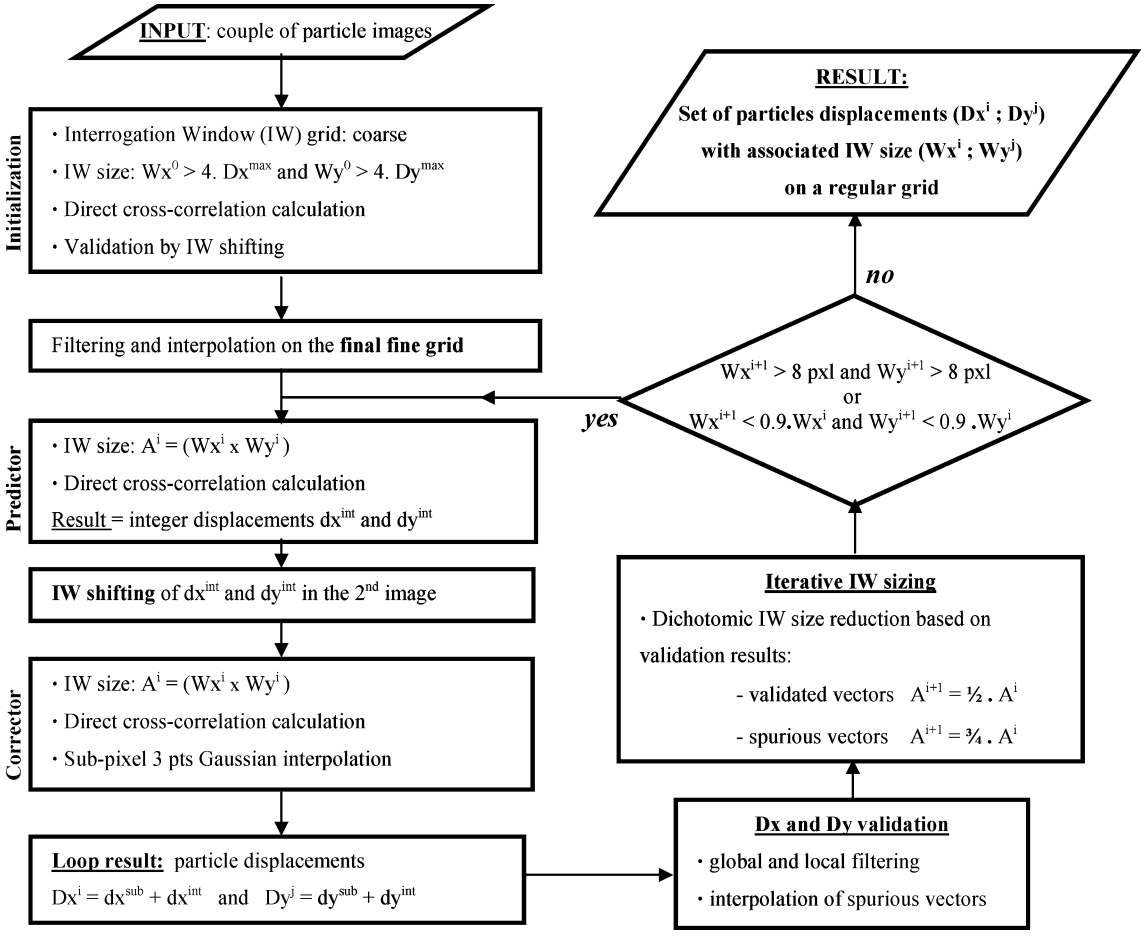

Fig. 6 Global diagram of the iterative algorithm

enables inhomogeneities of local particle density to take into account as observed in turbulent flows with internal recirculation zones (Susset et al. 1998). Indeed, the ability to use large IW in low particle concentration regions and to reduce size of the IW in high concentration zones enables an increase of the spatial resolution in the latter regions without losing the possibility of PIV measurements in the first regions. At the end of the iterative processing, two additional parameters, representing the final IW size, are stored with each displacement measurement.

4.2 Precision of the iterative processing for velocity gradient resolution

A set of synthetic images for different displacement gradients is again used to evaluate the iterative processing efficiency. The measured displacement gradient S_{mes} obtained by the iterative processing is also reported in Fig. 4. The slope of the linear regression is closer to 1 than the standard processing one. The gap between the two processing increases with the gradient values ($S_{imp} > 0.3$). The RMS values for the iterative processing is globally three times lower than the standard one. This last result shows that this new processing seems well adapted to large gradient resolution. Moreover, the final average size of IW (9×9 pixel^2) shows also that the independent sizing of the IW induces a better spatial resolution of the PIV measurements.

5 The super-resolution processing

The minimum size of the IW is fixed to 8×8 pixel^2 by the iterative processing. A better spatial resolution must be obtained by calculation of a displacement for each individual particle. For this, a super-resolution algorithm has been developed as a hybrid PIV/PTV method. The result of the iterative PIV processing becomes the input of the PTV procedure. The last processing steps consist of the detection of the particles in images, the interpolation of the PIV displacements on the detected particle positions and the matching of the particle pairs between the first and second images.

5.1 Particle detection in tomographic images

The detection of objects is a current operation in image processing and numerous algorithms are available but generally adapted to specific configurations (Carosone et al. 1995; Etoh et al. 1998). They usually include three stages: first the definition of the object properties in the

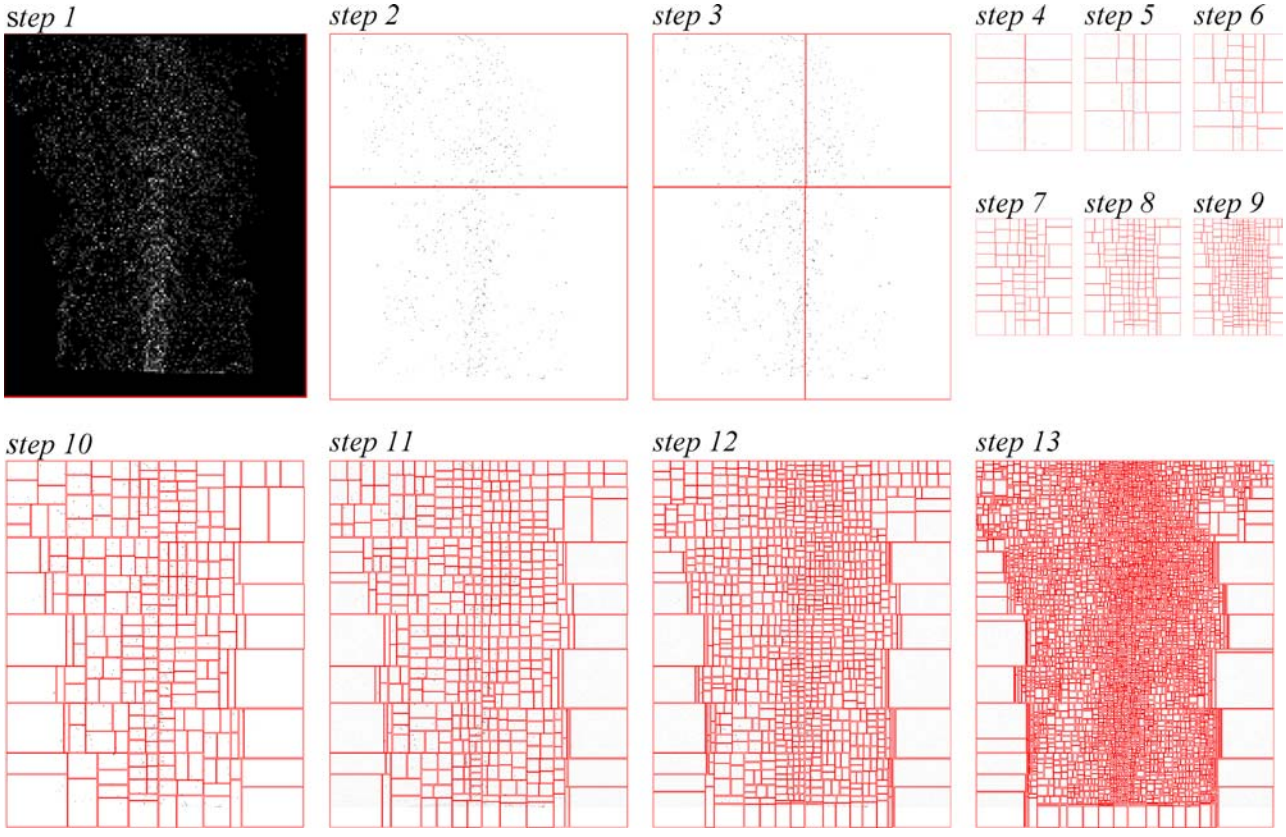

Fig. 7 Construction of a particle BSP from a real image containing 37,064 detected particles (the initial image is shown in step 1 and in reverse colours in other steps)

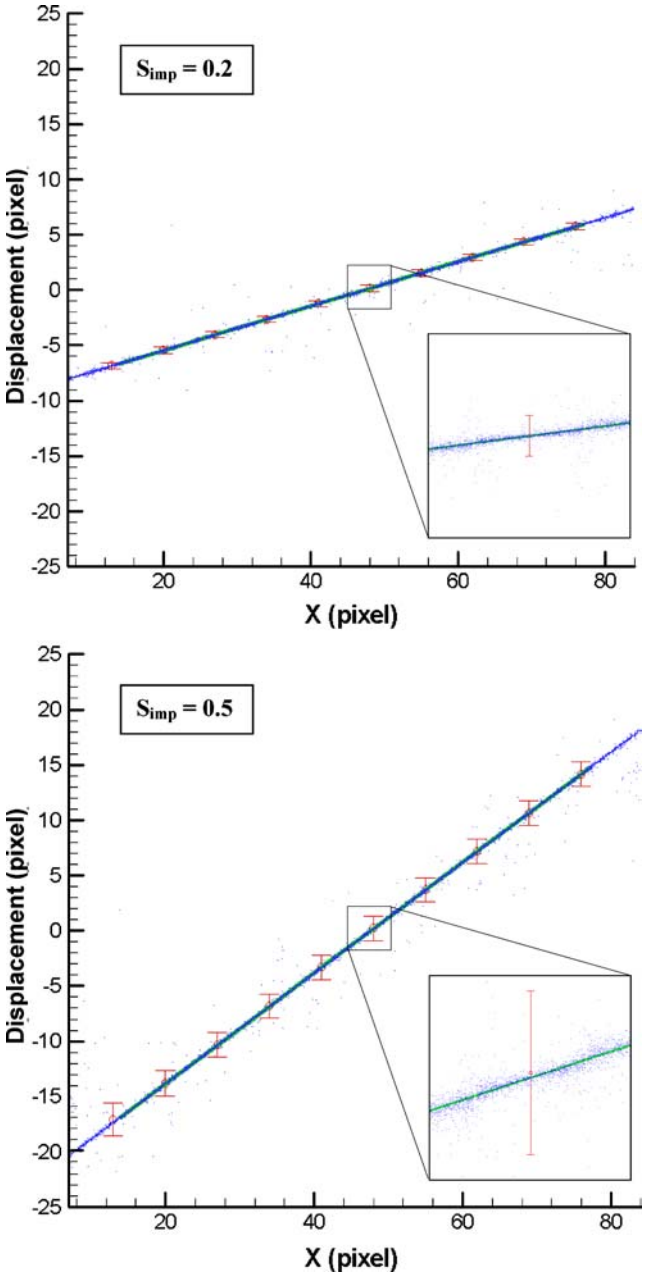

Fig. 8 Comparison of theoretical displacements (*line*) with results of iterative processing (*open circles and error bars*) and super-resolution processing (*dots*)

image: shape, size and intensity; second homogenisation of the image in order to get a quasi-constant object/background contrast; and third definition of thresholds to distinguish the object from the background. Our approach is based on particle elimination by an erosion operation in order to isolate them from the background of the image. For each analysis window, this operation attributes the minimum grey level value of the window to the centre pixel position. In the present case, the size of the erosion windows varies from 3×3 to 7×7 pixel^2. The resulting image is considered as the background reference. The RMS value of the intensity is then calculated in the background image in order to define a threshold corresponding to the addition of the local background signal and three times the RMS value. For each raw image pixel, if the grey level is superior to the threshold, the pixel is flagged as a signal. Then, the neighboured flagged pixels are analyzed to find the local intensity maximum. At this position, a Gaussian interpolation is used to establish the sub-pixel position, intensity amplitude and half-width size of the detected particle.

5.2 Data storage in binary space partition

With the super-resolution algorithm, the computational time for the interpolation procedure and the particle pairing can be very high when many of particles are present together in the tomographic images. In the present work, a new concept of data storage has been implemented, by the use of binary space partition (BSP) (De Berg et al. 2000). This concept has been developed for optimization of number of polygons processed by graphics processors (Fuchs et al. 1980), and is nowadays generally used in real-time animations of virtual world and 3D games (Watt and Policarpo 2000). The principle of BSP trees consists of an iterative space splitting in hierarchical planes. At each step, two space partitions are defined containing one half of the polygons of the previous iterative step. Then, the virtual world is defined as a succession of boxes hierarchically interlocked. In the present study, this principle has been adapted for filing the large number of particles detected. The particle BSP is constructed by successive images splitting in order to define two child leaves each containing the half of the particles of the mother leaf. The hierarchical subdivision is stopped when a minimum of ten particles is reached in the leaf. Figure 7 presents 13 successive steps of the construction of the particle BSP processed from a real image of a turbulent flow where 37,064 particles were detected. The main advantage of this BSP structure is a strong decrease in operations to localize a particle in the image and of the particle closest to a given position. For that, the particle BSP is scanned from the root node to the final leaves. At each BSP node, only one single test is needed to head to the leaf, the space being divided into two equivalent regions.

5.3 Interpolation of PIV displacements on particle positions

An interpolation of the displacement field obtained by the iterative processing on the particle positions is required to assign a displacement to each particle. A vector BSP is formed from the displacement field to accelerate this processing. Each final leaf contains, in a box, the calculated displacement at each four corners. For each particle, the interpolation step consists to search the vector BSP leaf including the particle. The displacement is then calculated from the four values at

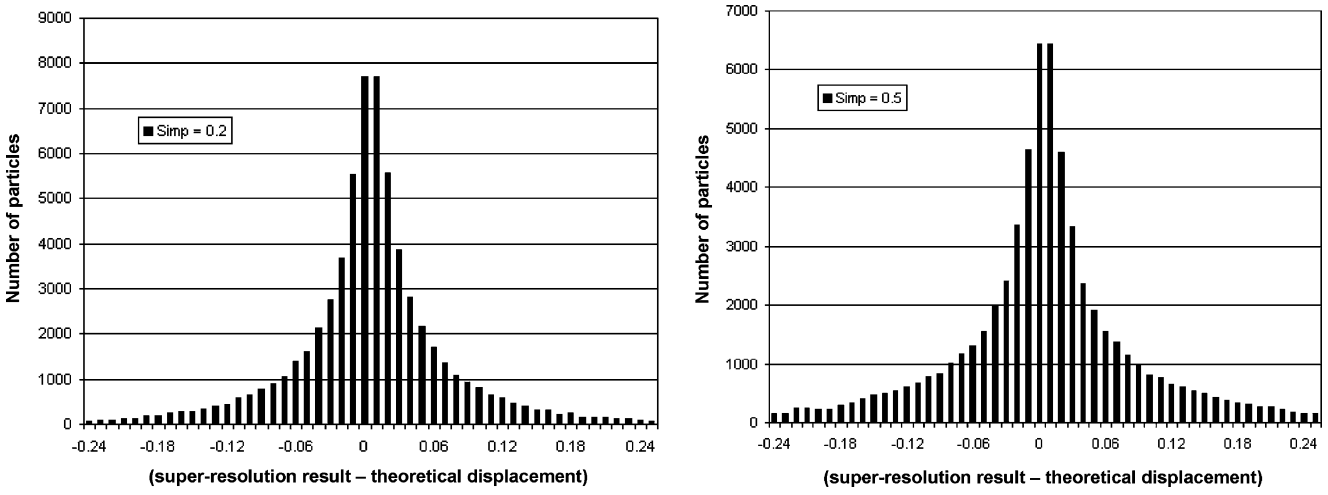

Fig. 9 Histograms of the difference between super-resolution result and theoretical displacement

Table 1 Successive steps of the super-resolution calculation of the real image on Fig. 7

Step	Parameters	Time (ms)
Particle detection in the first image	37,064 particles	202
Particle detection in the second image	38,488 particles	214
Construction of Particle BSP	13 successive steps	348
Construction of Vector BSP	101×74 displacements	66
Displacement interpolation	37,064 interpolations	69
Particle pair matching	36,470 pairs matched	1,548

the corners weighted by their distance to the particle position.

5.4 Matching of particle pairs

The last step of the super-resolution algorithm consists of the search for the particle in the second image corresponding to each particle in the first. This is done by first predicting the location of the particle in the second image through an interpolated position shift relative to the first image, and then by identifying the particle in the second image closest to the predicted location. For that, a window centred on the predicted position is defined in the second image with a shape and a size dependent of the displacement direction, the local displacement gradient and of the particle size. When several particles are present in the investigated window, the closest particle is selected. Finally, the resulting displacement is the difference between first and second image particle positions.

5.5 Computer time of super-resolution algorithm

Table 1 presents the main computational time characteristics of the successive steps of the super-resolution algorithm (1.2 GHz processor) on the real image shown in Fig. 7.

The total processing time is 2,447 ms for more than 15,000 vectors/s. The computational time for the PIV iterative processing for 7,474 displacements is 30 seconds, determined from an initialisation standard calculation in 30×50 pixel^2 IW and 9×9 pixel^2 final IW after ten iterations. This statistic shows that the super-resolution calculation represents only 10% of the complete processing duration. For the three steps (standard, iterative and super-resolution), 1,000 vectors/s can be calculated. This allows the use of such a super-resolution algorithm for a large number of velocity fields.

5.6 Resolution of velocity gradient and precision of the super-resolution processing

The results of the super-resolution algorithm are obtained on a non-regular grid while PIV algorithms work on regular fields. This complicates the comparison of the two approaches. A direct interpolation of discontinuous results on a regular grid may bias the precision analysis by inducing additive effects. To evaluate the precision, a statistical analysis is performed on super-resolution displacement fields obtained from synthetic images for different displacement gradients. For each displacement gradient S_{imp} value, more than 300,000 particles are detected and matched. Figure 8 gathers theoretical displacements (solid line), results of iterative processing (open circles), their corresponding RMS values (error bars), and super-resolution results (dots). Only 6,000 super-resolution results are presented for the legibility of the figure.

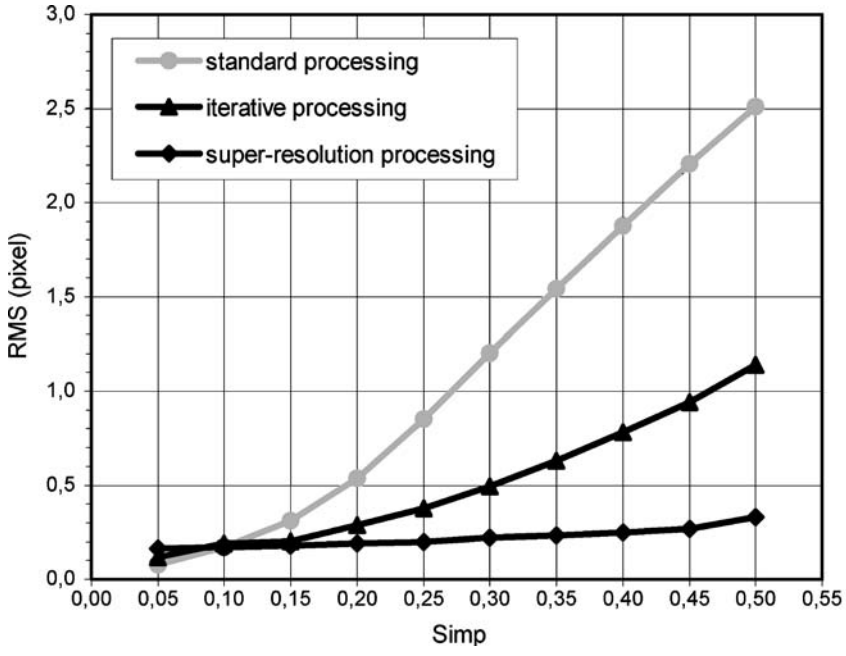

Fig. 10 Measurement errors of the standard, iterative and super-resolution processings versus imposed displacement gradient

It can be seen that the errors of the iterative processing notably increase with the gradient value, whereas the super-resolution result distributions seem to be constant and superimposed on the theoretical lines. A comparison of the super-resolution results and the theoretical displacement is reported in Fig. 9 for each S_{imp} value.

The distributions, centred on the zero value, keep a similar morphology for all gradient values. From these histograms, the measurement error of the super-resolution algorithm is defined as the value of a difference of 95% of the results. Figure 10 shows the obtained variation of the measurement error as function of the displacement gradient.

A small increase of the measurement error is still observed with S_{imp} with the same order of magnitude as for an uniform translation (Susset et al. 2000). Theoretically, the super-resolution measurement error can be split up into an error in particle position and in particle pair matching. The latter includes the iterative measurement, and the error in the choice of the corresponding particle in the second image. Nevertheless, the measurement error stays always inferior to 0.35 pixel which corresponds to twice the position error of the particles in the synthetic images. This super-resolution algorithm has been applied on time resolved PIV experiment on a bluff body turbulent flame (Susset et al. 2002) as well as in the framework of the second international PIV Challenge (Stanislas et al. 2005).

6 Conclusions

In this work, three different particle image processing methods have been presented for velocity measurement by PIV based on direct CC calculation . The limitations of the standard algorithm are pointed out for flows with large velocity gradients. To improve measurements, an iterative processing has been developed using a direct CC calculation with a great flexibility in the choice of the size and the shape of the interrogation window. The independent iterative reduction of the IW size at each location allows to take into account local particle concentration characteristics. The result shows the ability of the iterative processing on synthetic images to characterize large velocity gradient flows.

Enhancement of accuracy and spatial resolution have been obtained, thanks to a super-resolution algorithm which determines a displacement for each particle. The selected method for particle detection in tomographic images avoids any subjective criteria. However, this approach is not universal and it can sometimes be necessary to adapt the detection parameters to specific characteristics of each experiment. The use of binary space partition (BSP) structure permits a decrease in computational time allowing the use of a super-resolution algorithm on a large number of images. The precision of the velocity field is evaluated from synthetic images with large displacement gradients. The errors are minimal and are mainly connected to the determination of the particle position. The non-regular grids of the super-resolution results require the development of specific validation algorithms, e.g. neuronal networks, and the adaptation of post-processing tools for the determination of the derived parameters and for the statistical and spectral analysis.

Acknowledgements Authors wish to thank the Poitou Charentes Regional Council and Gaz de France for their financial support of a part of this work.

References

Carosone F, Cenedese A, Querzoli G (1995) Recognition of partially overlapped particles using the kohonen neural network. Exp Fluids 19:225–232

De Berg M, Van Kreveld M, Overmars M, Schwarzkopf O (2000) Computational geometry. Algorithms and applications. Springer, Berlin Heidelberg New York

Etoh T, Takehara K, Okamoto K (1998) The particle mask correlation method In: 8th symposium on flow visualisation. Sorrento, Italy

Fuchs H, Kedem ZM, Naylor BF (1980) On visible surface generation by a priori tree structures. In: Proceedings of the 7th annual conference on computer graphics and interactive techniques, Seattle, Washington, USA

Hart DP (1998) High speed PIV analysis using compressed image correlation. J Fluids Eng 120:463–470

Honoré D, Lecordier B, Susset A, Jaffré D, Perrin M, Most JM, Trinité M (2000) Time resolved Particle Image Velocimetry in confined Bluff-Body burner flames. Exp Fluids 29:S248–S254

Huang HT, Fiedler HE, Wang JJ (1993) Limitation and improvement of PIV—part I: limitation of conventional techniques due to deformation of particle images patterns. Exp Fluids 15:168–174

Huang HT, Fiedler HE, Wang JJ (1993) Limitation and improvement of PIV part II: particle image distorsion, a novel technique. Exp Fluids 15:263–273

Ishikawa M, Murai Y, Wada A, Iguchi M, Okamoto K, Yamamoto F (2000) A novel algorithm for particle tracking velocimetry using the velocity gradient tensor. Exp Fluids 29:519–531

Lecordier B (1997) Etude de l'interaction de la propagation d'une flamme prémélangée avec le champ aérodynamique, par association de la tomographie laser et de la vélocimétrie par images de particules. PhD Thesis, Université de Rouen

Quénot GM (2000) Vélocimétrie par images de particules stéréo par programmation dynamique. In: 7ème Congrès Francophone de Vélocimétrie Laser, Marseille, France

Quénot GM, Pakleza J, Kowalewski T (1998) Particle image velocimetry with optical flow. Exp Fluids 25:177–189

Roth GI, Katz J (2001) Five techniques for increasing the speed and accuracy of PIV interrogation. Meas Sci Technol 12:238–245

Sacarano F, Riethmuller ML (1999) Iterative multigrid approach in PIV image processing with discrete window offset. Exp Fluids 26:513–523

Stanislas M, Okamoto K, Kähler CJ, Westerweel J (2005) Main results of the second international PIV Challenge. Spec Issue Exp Fluids (To appear)

Susset A, Trinité M, Honoré D, Jaffré D, Perrin M (1998) Experimental investigation of spatio-temporal correlation between aerodynamic and flame front location in an axisymetric non premixed Bluff-Body burner flame. In: 9th International symposium on application of laser techniques to fluid mechanics, Lisbon, Portugal

Susset A, Most JM, Honoré D, Perrin M (2000) Développement d'un traitement itératif par corrélation directe pour l'application de la PIV aux écoulements à forts gradients de vitesse. In: 7ème Congrès Francophone de Vélocimétrie Laser, Marseille, France

Susset A, Most JM, Honoré D, Lecordier B, Trinité M (2002) Suivi temporel d'une flamme de brûleur Bluff-Body par PIV haute cadence. In: 8ème Congrès Francophone de Vélocimétrie Laser, Meudon, France

Susset A (2002) Développement de traitements d'images pour l'étude de la stabilisation de flammes turbulentes non-prémélangées générées par des brûleurs industriels modèles. PhD Thesis, Université de Poitiers

Tokumaru PT, Dimotakis PE (1995) Image correlation velocimetry. Exp Fluids 19:1–15

Watt A., Policarpo F (2000) 3D Games. Real-time rendering and software technology, vol 1. Addison Wesley, Reading